

LEAD: Layer-wise Expert-aligned Decoding for Faithful Radiology Report Generation

Ruixiao Yang^{♦♣}, Yuanhe Tian^{♥♣} Xu Yang[♦] Huiqi Li[♦] Yan Song[♣]

[♦]Beijing Institute of Technology [♣]Zhongguancun Academy

[♥]Zhongguancun Institute of Artificial Intelligence [♣]University of Science and Technology of China

[♦]{3220245229, pyro_yangxu, huiqili}@bit.edu.cn

[♥]tianyuanhe@zgci.ac.cn [♣]clksong@gmail.com

Abstract

Radiology Report Generation (RRG) aims to produce accurate and coherent diagnostics from medical images. Although large vision language models (LVLM) improve report fluency and accuracy, they exhibit hallucinations, generating plausible yet image-ungrounded pathological details. Existing methods primarily rely on external knowledge guidance to facilitate the alignment between generated text and visual information. However, these approaches often ignore the inherent decoding priors and vision-language alignment biases in pretrained models and lack robustness due to reliance on constructed guidance. In this paper, we propose Layer-wise Expert-aligned Decoding (LEAD), a novel method to inherently modify the LVLM decoding trajectory. A multiple experts module is designed for extracting distinct pathological features which are integrated into each decoder layer via a gating mechanism. This layer-wise architecture enables the LLM to consult expert features at every inference step via a learned gating function, thereby dynamically rectifying decoding biases and steering the generation toward factual consistency. Experiments conducted on multiple public datasets demonstrate that the LEAD method yields effective improvements in clinical accuracy metrics and mitigates hallucinations while preserving high generation quality.

1. Introduction

Radiology Report Generation (RRG) is a significant cross-modal task that bridges medical imaging and natural language processing, with the aim of automatically producing accurate, coherent and clinically informative textual descriptions for given radiological images (e.g. chest X-rays) (Sloan et al., 2024; Huang et al., 2025; Tian et al.,

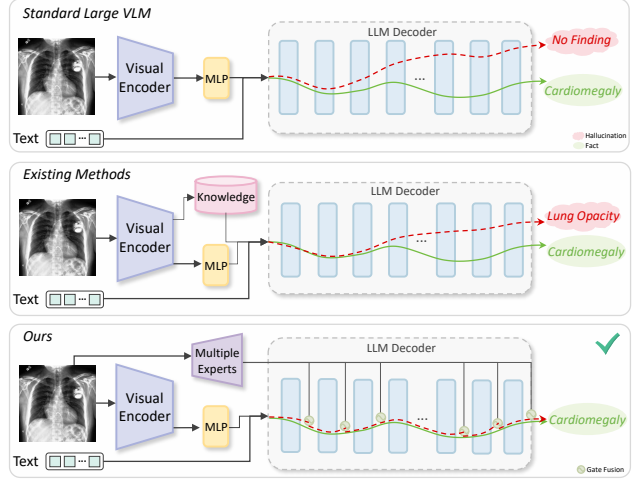


Figure 1. Conceptual illustration of Layer-wise Expert-aligned Decoding (LEAD). Unlike standard VLMs and existing methods that often succumb to intrinsic language priors (top and middle rows), our approach directly intervenes in the internal decoding process. By adaptively injecting fine-grained visual expert signals into intermediate representations of each decoder layer, LEAD dynamically rectifies the generation trajectory to ensure faithful alignment with fine-grained medical visual facts (bottom row).

2025). This technique can substantially reduce radiologists' workload and improve diagnostic efficiency, and can also act as an effective decision-support tool in resource-limited clinical settings (Johnson et al., 2019; Chen et al., 2020). With the rapid advancement of deep learning, especially Transformer architectures and large language models (LLMs), the RRG field has achieved remarkable progress, with the generated report fluency approaching human expert levels (Tu et al., 2024; Liu et al., 2025b). Existing RRG methods still face substantial challenges in achieving high clinical accuracy and maintaining factual consistency with the images. Recently, approaches based on vision-language models (VLM) have attempted to leverage the strong commonsense reasoning and language generation capabilities of LLMs to improve report quality, and have achieved no-

table performance gains (Li et al., 2023; Tian & Song, 2025; Tanno et al., 2025). Despite their strong performance in report generation and human acceptability, these methods still suffer from prominent hallucinations, where generated descriptions contradict imaging evidence (Kapadnis et al., 2024; Gu et al., 2025; Hou et al., 2025).

Hallucination is a common issue in VLMs, arising primarily from factors such as unbalanced and insufficient image–text matching data distributions, suboptimal cross-modal alignment between visual and textual representations, and the intrinsic language priors of LLMs (Liu et al., 2024b; Li et al., 2025). In medical image report generation, this issue largely degrades clinical accuracy and factual consistency. Specifically, hallucinations appear as misalignment between generated reports and fine-grained pathological findings in radiological images, causing factual inaccuracies (Huang et al., 2023; Gu et al., 2025; Jiang et al., 2025). Although existing studies have attempted to enhance the attention of VLMs to visual features and achieve fine-grained image–text alignment through various approaches (Liu et al., 2025b; Sun et al., 2025; Gu et al., 2025; Hou et al., 2025) to improve report accuracy, most adhere to a common paradigm: constructing knowledge bases from relevant fine-grained visual–textual information, and subsequently utilizing retrieval-augmented (RAG) or contrastive learning to provide alignment guidance during report generation via optimization at the prompt or token level. However, these approaches overlook addressing hallucinations from their intrinsic causes in VLMs. Though such guidance improves output accuracy, the models still suffer from decoding and alignment biases induced by the inherent prior knowledge of pretrained LLMs. Furthermore, this design induces heavy reliance on constructed guidance, where any bias therein is propagated to generated reports, ultimately compromising model robustness. Therefore, addressing inherent decoding and alignment biases to mitigate hallucinations at the source is a crucial research direction, as it enables more accurate alignment between fine-grained visual features and textual semantics and leads to more robust and factually consistent report generation models.

To address these limitations, we propose Layer-wise Expert-aligned Decoding (LEAD), which injects fine-grained visual expert signals into the VLM decoding process using multi-label pathological classification features extracted from medical images. This design aims to mitigate hallucinations and enforce tighter alignment between generated reports and visual evidence, as shown in Figure 1. LEAD is inspired by recent VLM studies that reduce LLM priors decoding biases by injecting statical perturbations into intermediate decoder representations during inference (Su et al., 2025b; Wu et al., 2025; Chen et al., 2025). Unlike these methods, our approach requires an adaptive injection strategy to integrate expert signals which are inherently rich in effective

information and diverse across samples. Our objective is to dynamically incorporate these signals into intermediate representations to achieve fine-grained visual alignment. We conceptualize the VLM as a knowledgeable yet error-prone “student” guided by “visual experts”, mirroring an iterative refinement process. Concretely, each decoding layer is treated as a generation step, where projected expert features are selectively fused into intermediate representations via a context-aware gated fusion mechanism. This guides the decoding trajectory toward a low-hallucination trajectory by utilizing fine-grained visual cues, thereby suppressing LLM prior bias. Furthermore, lightweight unfreezing and fine-tuning during this process enhance visual–textual semantic alignment through direct interaction between the LLM and expert signals. Compared with methods based on fixed perturbations or external knowledge bases, LEAD shows superior adaptability and robustness while effectively suppressing hallucinated content unrelated to visual evidence.

This work makes the following contributions:

- We propose Layer-wise Expert-aligned Decoding, a novel framework that uses multi-label pathological features as visual expert signals to rectify the intrinsic decoding priors of LLM. By strategically injecting these signals into each decoder layer, our method ensures the generated reports adhere closely to visual evidence.
- We design a bidirectional integration mechanism that treats report generation as an interactive expert-guided process, employing a context-aware gated fusion mechanism at each decoding layer to adaptively integrate fine-grained expert signals. This facilitates a dynamic shift in the decoding trajectory toward visual facts.
- Experiments on both the CheXpert Plus and MIMIC-CXR datasets demonstrate that our approach substantially improves clinical accuracy, effectively reducing hallucinations while preserving report fluency.

2. The Approach

This work presents a novel layer-wise expert-aligned decoding framework for radiology report generation, built upon the Qwen3-VL architecture. An overview of the proposed framework is illustrated in Figure 2. To mitigate hallucinations, LEAD injects fine-grained visual expert signals directly into the decoding process. By enabling each LLM layer to selectively integrate these signals into intermediate representations, the framework dynamically steers the decoding trajectory toward visual facts. Specifically, we design a visual expert module consisting of pathology-specific classifiers to capture comprehensive fine-grained features. These expert signals undergo distinct projections when injected into different decoder layers to transform into appropriate information for each layer. Meanwhile, the decoder

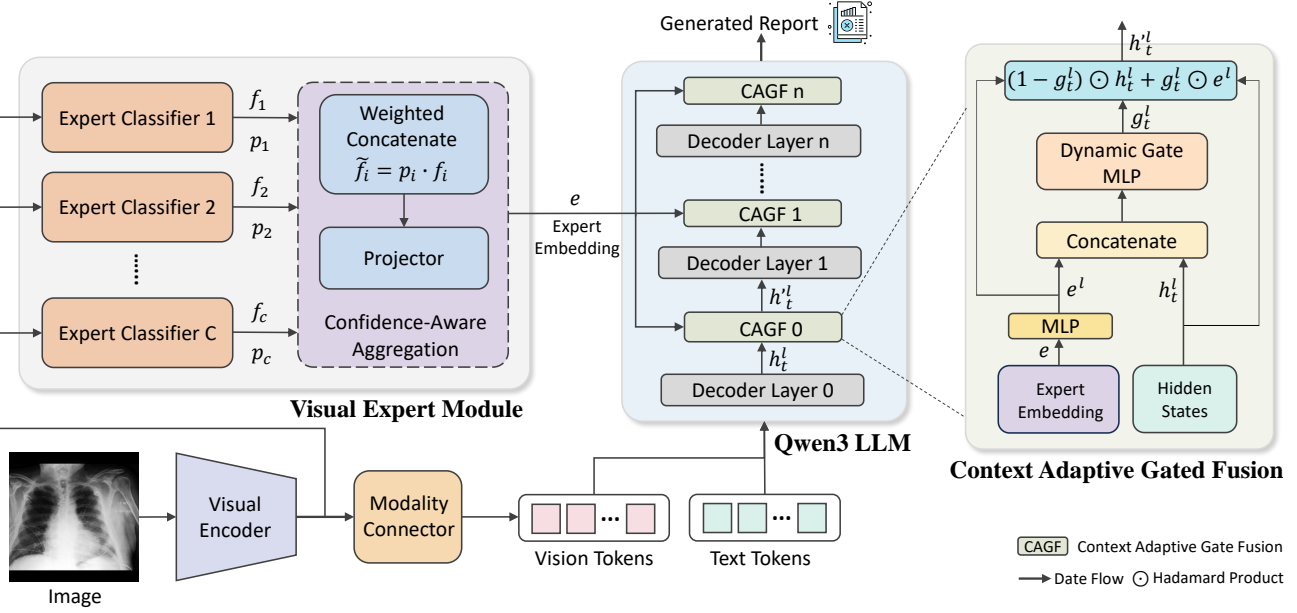


Figure 2. An overview of the proposed framework.

employs a context-aware gated fusion mechanism to adaptively absorb expert information at each layer, effectively rectifying decoding biases derived from LLM priors and enhancing the clinical accuracy of the generated reports.

2.1. Backbone

An appropriate backbone is essential for the proposed method, as RRG requires a VLM that combines advanced LLM capabilities with strong cross-modal understanding. This backbone not only enables high-quality report generation, but also provides a solid foundation to further improve image–text alignment and hallucination suppression. We adopt Qwen3-VL as the backbone due to its strong multimodal comprehension and text generation capabilities.

Qwen3-VL is a state-of-the-art VLM that integrates a ViT visual encoder, a modality connector based on multilayer perceptron (MLP), and the Qwen3 large language model (Bai et al., 2025). Given a radiological image, the visual encoder extracts a sequence of embeddings, which are aligned into the language token space and concatenated with prompt tokens for decoding. To balance training efficiency with the preservation of pretrained knowledge, we employ a hybrid fine-tuning strategy. We apply Low-Rank Adaptation (LoRA) (Hu et al., 2022) to the LLM’s attention weights while freezing its core parameters to prevent catastrophic forgetting. Concurrently, the visual encoder and our proposed modules are fully fine-tuned to capture domain-specific medical patterns and facilitate visual-textual alignment.

2.2. Visual Expert Module

To extract pathological visual features and leverage them to guide text decoding, we integrate a visual expert branch. The module comprises a set of specialized experts corresponding one-to-one with target categories, where each is instantiated as a three-layer MLP binary classifier. During forward propagation, we replicate feature maps from the final layer of the visual encoder to feed this expert branch. Supervised by pathological labels extracted from reports (e.g., cardiomegaly, pleural effusion), experts learn to capture discriminative features indicative of specific pathological conditions. The intermediate features from each classifier are then concatenated to construct a comprehensive expert embedding. Subsequently, these signals are incorporated into the LLM decoding process through a fusion mechanism described in the following section, enabling factually grounded visual evidence to guide hallucination mitigation.

2.3. Layer-wise Expert-Aligned Decoding Method

To effectively bridge the gap between visual evidence and textual generation, we propose the LEAD method. This method is designed to simulate a continuous “consultation” process where the language model like a student actively interacts with the pathological classifiers like experts at each step of the generation process. Unlike existing methods restricted to input level knowledge injection or fixed pattern interventions, our approach orchestrates a bidirectional interaction at each decoding layer by adaptively embedding expert guidance and enabling the decoder to perform a secondary selection of these signals. This mechanism

steers intermediate representations closer to visual evidence, progressively correcting decoding deviations to suppress hallucinations and ensure factual consistency of reports.

2.3.1. CONFIDENCE-AWARE EXPERT AGGREGATION

To achieve adaptive integration of expert signals tailored to diverse input samples, we employ a confidence-aware fusion strategy. Recognizing that pathological manifestations vary between different cases, we modulate the feature vector \mathbf{f}_i of each expert by its confidence score $p_i = \sigma(s_i)$, where s_i denotes the classification logit and σ denotes the sigmoid. This operation, formulated as $\tilde{\mathbf{f}}_i = p_i \cdot \mathbf{f}_i$, effectively suppresses the noise of irrelevant experts. The weighted features are then concatenated and linearly projected to form the global expert embedding $\mathbf{e} \in \mathbb{R}^d$, where d denotes the feature dimension of the intermediate representations.

2.3.2. ADAPTIVE EXPERT PROJECTION

Since different layers of the LLM decoder capture semantic information at varying levels, the visual expert signals must be adaptively transformed to align with the feature space of each layer. For the l -th layer of the decoder, we employ an MLP layer to produce the layer-wise expert embedding \mathbf{e}^l :

$$\mathbf{e}^l = \phi^l(\mathbf{e})$$

where $\phi^l(\cdot)$ represents the MLP transformation of the l -th layer. This transformation allows the module to adaptively emphasize specific pathological features relevant to the current depth of the decoding network architecture.

2.3.3. CONTEXT-ADAPTIVE GATED FUSION MECHANISM

To integrate the expert knowledge into the LLM, we introduce a gated fusion block at each decoder layer. The core motivation behind this design is to empower the decoder to selectively absorb visual evidence without disrupting the inherent semantic flow of the autoregressive generation. Instead of indiscriminately mixing multimodal features, which risks compromising the pretrained linguistic coherence, we employ a context-aware gated fusion mechanism combined with an interpolation connection. Note that the hidden state here corresponds to the intermediate representation referenced in our preceding discussion of the LEAD architecture.

Let $\mathbf{H}^l = \{\mathbf{h}_1^l, \dots, \mathbf{h}_T^l\}$ denote the sequence of hidden states in the l -th layer. Since the expert embedding \mathbf{e}^l contains global pathological information, we first expand it to match the sequence length of \mathbf{H}^l . At each step t of the sequence, we determine the injection intensity by checking both the current context and the visual signal. We concatenate the current hidden state \mathbf{h}_t^l with the expert embedding \mathbf{e}^l to compute a dynamic gate g_t^l :

$$\mathbf{g}_t^l = \sigma(\phi_{gate}([\mathbf{h}_t^l; \mathbf{e}^l])) \quad (1)$$

where $[\cdot; \cdot]$ represents the concatenation operation. The expert signals is then injected via an interpolation connection:

$$\mathbf{h}'_t^l = (1 - \mathbf{g}_t^l) \odot \mathbf{h}_t^l + \mathbf{g}_t^l \odot \mathbf{e}^l \quad (2)$$

where \odot represents the Hadamard product. This mechanism functions as a soft selection switch: if the current hidden state \mathbf{h}_t^l correlates with the generation of text grounded in visual facts, the gate opens to incorporate the relevant expert information; conversely, if \mathbf{h}_t^l pertains to content unrelated to visual input, the gate value remains suppressed to preserve the original linguistic fluency. This effectively steers the intermediate representations toward a decoding trajectory aligned with visual facts, thereby suppressing hallucinations induced by the LLM’s priors and promoting alignment between the generated text and visual evidence.

2.4. Training Strategy

Training a robust RRG model requires balancing the retention of the LLM’s linguistic fluency with the acquisition of domain-specific medical visual understanding. To achieve this, we employ a fine-tuning strategy combined with a multi-task objective to optimize the overall performance.

We freeze the majority of the LLM parameters to preserve pre-trained capabilities, while fine-tuning the model via LoRA for efficient domain adaptation. Concurrently, to ensure the extraction of pathological features, we fully unfreeze the vision encoder, the modality connector, the proposed Visual Expert Module, and all layer-wise expert-aligned decoding blocks. This allows the visual backbone to learn fine-grained pathological representations while the injection modules learn the optimal alignment strategy.

Training is supervised by a composite loss function \mathcal{L} combining of the generation loss and the pathological classification loss. The generation task is optimized via standard Cross-Entropy loss (\mathcal{L}_{gen}) for next-token prediction:

$$\mathcal{L}_{gen} = - \sum_{t=1}^T \log P(y_t | y_{<t}, \mathbf{I}) \quad (3)$$

where y_t is the target token and \mathbf{I} is the image. Simultaneously, to ensure the expert module provides accurate guidance, we apply a multi-label Binary Cross-Entropy loss (\mathcal{L}_{cls}) to the predictions of the expert classifiers:

$$\mathcal{L}_{cls} = - \sum_{i=1}^C [c_i \log(\hat{c}_i) + (1 - c_i) \log(1 - \hat{c}_i)] \quad (4)$$

where C is the number of pathology categories (experts), c_i is the ground-truth label extracted from the report, and \hat{c}_i is

Table 1. Dataset statistics.

DATASET	TRAINING	VAL	TESTING
CHEXPERT PLUS	40,463	5,780	11,562
MIMIC-CXR	270,790	2,130	3,858

the predicted probability. The total objective is a weighted sum of these terms to balance generation and classification:

$$\mathcal{L} = \mathcal{L}_{gen} + \lambda \mathcal{L}_{cls} \quad (5)$$

where λ is a hyperparameter balancing the two tasks. Based on empirical observations, we set $\lambda = 4$ to achieve a balance of magnitude between the losses. This configuration enforces explicit supervision on the visual experts, thereby ensuring that the injected signals are factually grounded.

3. Experiment Settings

3.1. Datasets

To conduct a comprehensive evaluation of our proposed framework, we primarily use the CheXpert Plus dataset (Chambon et al., 2024), a recently introduced large-scale benchmark for the generation of chest radiograph reports. Additionally, we employ the MIMIC-CXR dataset (Johnson et al., 2019) to conduct supplementary analytical experiments and assess the model’s generalization capabilities. The dataset partition is presented in Table 1.

CheXpert Plus. The dataset comprises approximately 220k chest X-rays paired with comprehensive radiology reports. Reports in CheXpert Plus are parsed into structured sections, such as Indication, Findings and Impression, while also including detailed patient demographics and labels for 14 pathology categories extracted via CheXBert (Smit et al., 2020). We adopted the data filtering and partitioning protocols as defined in CXPMRG-Bench (Wang et al., 2025a). Specifically, we retained samples with findings sections, resulting in a corpus of 57,805 image-report pairs. The dataset was then randomly divided into training, validation, and testing sets following the 7:1:2 ratio.

MIMIC-CXR. The MIMIC-CXR dataset serves as a standard benchmark in the field, consisting of 377,110 chest radiographs and 227,827 free-text radiology reports. In this work, we utilize a subset of the MIMIC-CXR dataset to conduct supplementary analytical experiments. This enables us to validate the generalization capability of our method across different clinical data distributions.

3.2. Baseline

To evaluate the effectiveness of LEAD, we conduct a comprehensive comparison on the CheXpert Plus dataset with representative methods spanning the field’s evolution. We benchmark a diverse range of baselines, ranging

from classical Transformer architectures, including R2Gen (Chen et al., 2020), R2GenCMN (Chen et al., 2021), and R2GenRL (Qin & Song, 2022), to early generative models like CvT2DistilGPT2 (Nicolson et al., 2023). Furthermore, we compare with recent advanced large VLMs, R2GenGPT (Wang et al., 2023) equipped with Llama2 (Touvron et al., 2023) and Llama3 (Grattafiori et al., 2024), the retrieval-augmented R2GenCSR (Wang et al., 2024), and the Mamba-based MambaXray-VL (Wang et al., 2025a).

To validate the effectiveness and adaptability of LEAD, we conduct comprehensive internal comparisons using the Qwen3-VL backbone, which is the latest version of Qwen series models that achieve state-of-the-art performance on many tasks (Liu et al., 2025a; Zhang et al., 2025; Deng & Mihalcea, 2025; Su et al., 2025a; Bai et al., 2025; Chen et al., 2026; Wang et al., 2026) We design controlled experiments across four distinct configurations: fully frozen parameters, standard LoRA fine-tuning (Hu et al., 2022), fine-tuning the vision tower only, and a hybrid strategy. In each setting, the corresponding vanilla model serves as the control to quantify the incremental performance gains. Furthermore, we investigate scalability by evaluating models with 2B, 4B, and 8B parameters for comprehensive validation.

3.3. Implementation Details

We implement our proposed framework using PyTorch and the Hugging Face Transformers library. All experiments are conducted on 2 NVIDIA A100 (80GB) GPUs.

Model Configuration. We employ Qwen3-VL-Instruct as the backbone and conduct experiments across three scales: 2B, 4B, and 8B. To efficiently adapt the model while preserving pre-trained knowledge, we apply Low-Rank Adaptation (LoRA) to all linear layers within the LLM’s attention and feed-forward networks ($r = 64$, $\alpha = 128$).

Training Strategy. The model is trained for 8 epochs with a total batch size of 16 and a gradient accumulation step of 4. We use the AdamW optimizer with a peak learning rate of 2e-4. A cosine annealing scheduler is employed for learning rate decay, accompanied by a linear warmup for the first 3% of training steps. For input processing, all images are resized to a resolution of 256×256 pixels. During the inference phase, we employ greedy decoding to generate radiology reports, prioritizing the most probable tokens.

Evaluation Metrics. We employ a comprehensive set of metrics to assess both the linguistic quality and clinical correctness of the generated reports. For Natural Language Generation (NLG) performance, we report ROUGE-L (Lin, 2004), METEOR (Banerjee & Lavie, 2005), and CIDEr (Vedantam et al., 2015), which measure the lexical overlap and semantic similarity between the generated text and ground-truth reports. To evaluate Clinical Efficacy (CE), we

Table 2. Comparison with the prior baselines on the CheXpert Plus Dataset. The evaluation metrics include Natural Language Generation scores (**R-L**: ROUGE-L, **M**: METEOR, **C**: CIDEr) and Clinical Efficacy scores (**P**: Precision, **R**: Recall, **F1**: F1-score) which are reported as macro-averages. **Bold** indicates the best performance overall, and underlined denotes the second best results.

METHOD	PUBLISH	DECODER	R-L	M	C	P	R	F1
R2GEN (CHEN ET AL., 2020)	EMNLP20	TRANSFORMER	0.246	0.113	0.077	0.318	0.200	0.181
R2GENCMN (CHEN ET AL., 2021)	ACL21	TRANSFORMER	0.256	0.127	0.102	<u>0.329</u>	0.241	0.231
R2GENRL (QIN & SONG, 2022)	ACL22	TRANSFORMER	0.186	0.101	0.012	0.193	0.229	0.196
CVT2DISTILGPT2 (NICOLSON ET AL., 2023)	AIM23	GPT2	0.238	0.118	0.101	0.285	0.252	0.246
R2GENGPT (WANG ET AL., 2023)	META-RAD,23	LLAMA2-7B	<u>0.266</u>	0.145	0.123	0.315	0.244	0.260
R2GENCSR (WANG ET AL., 2024)	ARXIV24	LLAMA3-8B	0.220	0.121	0.134	0.306	0.232	0.222
MAMBA ^X RAY-VL-B (WANG ET AL., 2025A)	CVPR25	LLAMA2-7B	0.265	<u>0.146</u>	0.121	0.315	0.247	0.259
LLAMA2-7B	0.267	0.149	0.117	0.333	<u>0.264</u>	0.273		
LAYER-WISE EXPERT-ALIGNED DECODING (LEAD)	OURS	QWEN3-2B	0.188	0.108	0.075	0.282	0.237	0.243
LAYER-WISE EXPERT-ALIGNED DECODING (LEAD)	OURS	QWEN3-4B	0.192	0.115	0.080	0.296	0.242	0.250
LAYER-WISE EXPERT-ALIGNED DECODING (LEAD)	OURS	QWEN3-8B	0.197	0.125	0.082	0.320	0.267	0.275

utilize the standard CheXpert labeler (Irvin et al., 2019) to extract labels for 14 prominent pathological observations from both generated and reference reports. By comparing these extracted labels, we compute Precision, Recall, and F1-score to quantify diagnostic accuracy. All CE metrics are reported as macro-averages to ensure balanced evaluation across all pathology categories regardless of their frequency.

4. Result and Analysis

To empirically validate the effectiveness of the proposed Layer-wise Expert-aligned Decoding (LEAD) framework, we conducted extensive experiments on the CheXpert Plus and MIMIC-CXR datasets. In this section, we provide a detailed analysis of performance comparison with state-of-the-art methods, the adaptability of our approach across different training configurations, and the contribution of individual components through ablation studies.

4.1. Comparison with Other Methods

We benchmark our proposed LEAD framework with comprehensive baselines, ranging from transformer architectures to contemporary large VLMs. The quantitative results on the CheXpert Plus dataset are summarized in Table 2.

The primary objective of LEAD is to rectify decoding biases and mitigate hallucinations inherent in large VLMs. As reported in Table 2, our method using Qwen3-8B achieves a clinical F1-score of 0.275, surpassing the performance of recent advanced models such as MambaXray-VL and the retrieval-augmented approach R2GenCSR.

Crucially, compared with recent RRG frameworks utilizing advanced LLM backbones, LEAD demonstrates a substantial margin in clinical accuracy. While existing approaches optimize visual encoders or employ instruction tuning, they often fail to suppress the LLM’s intrinsic tendency to generate unfounded findings driven by internal priors. This evidence suggests that relying solely on external interventions is insufficient to guarantee medical factuality. Instead,

our strategy of directly injecting fine-grained expert signals into decoding layers proves more effective, steering the generation trajectory toward visual consistency in real-time.

Regarding NLG metrics, we observe that LEAD yields slightly lower scores compared to other baselines. This phenomenon is expected, as standard metrics prioritize lexical overlap and often reward models that overfit to generic linguistic templates. However, LEAD encourages the decoder to adhere to fine-grained visual signals. This guides the model to generate clinically precise descriptions, effectively relaxing the strict alignment with the stylistic patterns of ground truth templates in favor of diagnostic accuracy.

We further investigate LEAD’s scalability across Qwen3 backbones (2B, 4B, 8B). As shown in Table 2, we observe a positive correlation between model capacity and diagnostic performance, suggesting that larger models better interpret and integrate the pathological constraints injected. Notably, even our lightweight 2B variant achieves an F1-score of 0.243, competitive with the larger R2GenGPT-Llama3-8B, confirming that LEAD’s effectiveness stems from its intrinsic alignment mechanism rather than parameter scaling.

4.2. Robustness and Generalization Analysis

To verify that the performance gains are intrinsic to the LEAD framework rather than dependent on specific fine-tuning strategies, we conducted controlled experiments across four distinct training configurations. It is important to note that in all settings, the parameters of the proposed LEAD module are fully trainable to learn the optimal alignment, regardless of whether the backbone is frozen or unfrozen. The comparative results are presented in Table 3.

To verify that performance gains are intrinsic to the LEAD framework rather than dependent on specific fine-tuning strategies, we conducted controlled experiments across four training configurations. The results demonstrate that LEAD consistently improves the F1-score of the backbone model across all settings. It is important to note that in all con-

Table 3. Effectiveness of LEAD under different settings. We compare the vanilla backbone with the backbone equipped with our LEAD method across four fine-tuning configurations on two datasets. The symbols \times and \checkmark denote frozen and trainable parameters, respectively. Note that the parameters of the proposed LEAD modules are fully trainable in all “Ours” settings.

MODEL	SETTINGS		CHEXPERT PLUS						MIMIC-CXR					
	VISION TOWER	LLM	R-L	M	C	P	R	F1	R-L	M	C	P	R	F1
BACKBONE	\times	\times	0.114	0.103	0.050	0.223	0.201	0.195	0.112	0.101	0.055	0.219	0.228	0.192
OURS	\times	\times	0.188	0.118	0.074	0.241	0.212	0.214	0.190	0.109	0.081	0.237	0.212	0.197
BACKBONE	\checkmark	\times	0.190	0.112	0.077	0.267	0.235	0.226	0.200	0.114	0.086	0.241	0.230	0.214
OURS	\checkmark	\times	0.193	0.118	0.077	0.278	0.245	0.241	0.202	0.118	0.093	0.262	0.238	0.225
BACKBONE	\times	\checkmark	0.192	0.115	0.076	0.265	0.239	0.228	0.198	0.114	0.089	0.248	0.228	0.217
OURS	\times	\checkmark	0.194	0.123	0.080	0.281	0.242	0.245	0.203	0.120	0.097	0.269	0.246	0.232
BACKBONE	\checkmark	\checkmark	0.191	0.119	0.079	0.270	0.241	0.243	0.202	0.117	0.093	0.280	0.242	0.231
OURS	\checkmark	\checkmark	0.197	0.125	0.082	0.320	0.267	0.275	0.208	0.120	0.104	0.298	0.250	0.247

Table 4. Ablation study on CheXpert Plus. “Exp.” indicates the presence of the visual expert module. “Proj.” denotes the projection strategy, where “Shared” uses a single projection shared across all layers and “Layer” uses distinct layer-wise projections. “Fuse.” represents the fusion mechanism, comparing our context-adaptive “Gate” with direct “Add”.

CONFIGURATION	EXP.	PROJ.	FUSE.	METRICS				
				R-L	M	C	P	R
-	-	-	-	0.191	0.119	0.079	0.270	0.241
\checkmark	-	-	-	0.189	0.118	0.075	0.268	0.244
\checkmark	SHARED	GATE	-	0.192	0.120	0.079	0.275	0.246
\checkmark	LAYER	ADD	-	0.194	0.123	0.080	0.295	0.253
\checkmark	LAYER	GATE	-	0.197	0.125	0.082	0.320	0.267
			0.275					

figurations, the parameters of the LEAD module are fully trainable to learn the optimal alignment. Specifically, in the most restricted scenario where both the vision tower and LLM are frozen, exclusively optimizing our inserted components boosts the F1-score from 0.195 to 0.214. This confirms that even when the backbone’s capacity is locked, our experts can extract and inject pathological cues that the frozen model fails to utilize. This advantage is further amplified in the fully optimized hybrid setting, where LEAD propels the performance from 0.243 to a peak of 0.275. The significant margin of +3.2% indicates that our layer-wise injection mechanism provides unique capabilities to continuously steer the decoding trajectory toward visual facts.

To assess the adaptability of the model, we extended the evaluation to the MIMIC-CXR dataset. The results mirror the trends observed on CheXpert Plus, with LEAD consistently outperforming the backbone across settings. This stability across datasets confirms that our framework captures robust pathological-textual alignments rather than overfitting to specific data distributions or training configurations.

4.3. Ablation Study

To validate the necessity of each component within the proposed LEAD framework, we conducted an ablation study on the CheXpert Plus dataset. The results are summarized

in Table 4. We first evaluate a variant that employs the visual expert module solely as an auxiliary classification task without injecting features into the decoder. The performance of this configuration is comparable to the baseline. This result suggests that merely optimizing a multi-task objective is insufficient to correct hallucinations.

When incorporating expert signals, sharing the output of a single projection across all layers yields a marginal performance improvement. However, a substantial gap remains when compared to our layer-wise projection strategy. This performance disparity validates our hypothesis that LLM decoding layers at varying depths capture different levels of semantic abstraction, thereby necessitating distinct, layer-specific expert projections rather than a uniform signal.

Finally, we analyze the fusion mechanism by replacing the dynamic gate with a direct “Add” operation. This leads to a suboptimal performance. The superior performance of our proposed method highlights the critical role of the context-adaptive gated fusion. This mechanism acts as a dynamic “soft switch” allowing the decoder to selectively integrate expert evidence only when relevant to the current generation step, thereby maximizing visual alignment without disrupting the linguistic coherence of the backbone.

4.4. Qualitative Analysis

To intuitively evaluate clinical accuracy, Figure 3 presents a qualitative comparison between the fully unfrozen hybrid fine-tuned baseline and our LEAD framework. As observed, the baseline model frequently suffers from factual inconsistencies and omissions. For example, it fails to detect pulmonary edema in the first case and hallucinates a “normal” heart size in the subsequent cases despite clear visual evidence of cardiomegaly. However, LEAD accurately rectifies these decoding biases by leveraging fine-grained expert signals. Our method not only successfully captures fine-grained pathological details missed by the backbone, such as pleural effusions in the second case, but also corrects hallucinated descriptions to accurately diagnose the enlarged

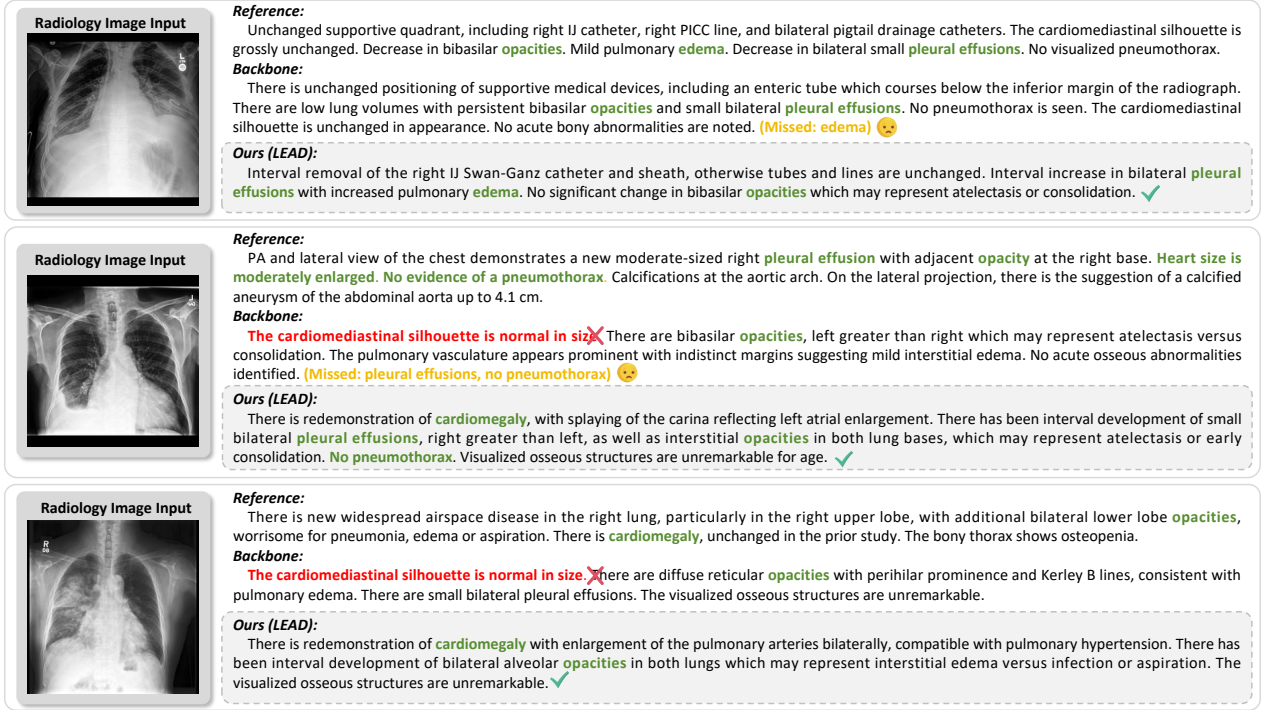


Figure 3. Qualitative comparison of generated reports. “Backbone” represents the results of the fully unfrozen hybrid fine-tuned backbone. Green text indicates correct pathological findings, red highlights factual errors, and yellow denotes missed findings.

heart. This qualitative evidence confirms that our layer-wise injection mechanism effectively steers the generation toward high clinical accuracy and aligns with visual facts.

5. Related Work

Large Vision-Language Models for RRG. The evolution of RRG has transitioned from early encoder-decoder architectures (Chen et al., 2021; Babar et al., 2021; Wang et al., 2025b) to Large Vision-Language Models (LVLMs) that leverage the reasoning capabilities of pretrained LLMs (Li et al., 2023; Tanno et al., 2025). Representative frameworks, such as R2GenGPT (Wang et al., 2023), employ lightweight adapters to align visual features with frozen LLMs. However, by treating the LLM as a black box, these methods remain vulnerable to intrinsic language priors. Consequently, they frequently generate hallucinations where descriptions deviate from fine-grained visual evidence (Liu et al., 2023; Tian et al., 2024; Kapadnis et al., 2024; Liu et al., 2024a; Gu et al., 2025; Hou et al., 2025).

Hallucination Mitigation Strategies. To address hallucinations, existing approaches primarily rely on external knowledge or auxiliary alignment objectives. This category includes Retrieval-augmented (RAG) (Wang et al., 2024; Liu et al., 2025b; Sun et al., 2025; Hou et al., 2025) and contrastive learning approaches (Gu et al., 2025; Wang et al., 2025b). While these techniques enhance image-text match-

ing, they share a limitation: they intervene largely at the prompt or token level via external guidance, overlooking the intrinsic decoding biases within the LLM. Furthermore, this reliance on constructed knowledge compromises model robustness when external guidance is suboptimal.

Decoding Intervention Methods. In the general domain, strategies such as activation steering have been explored to suppress hallucinations (Su et al., 2025b; Wu et al., 2025; Chen et al., 2025). However, these generic strategies typically rely on static interventions, lacking the fine-grained adaptivity required for complex pathological features.

Unlike previous methods, our LEAD framework introduces a dynamic, internal intervention mechanism. By integrating multi-label expert signals via layer-wise gated fusion, LEAD adaptively rectifies the decoding trajectory to align with visual facts, offering a solution to intrinsic model biases.

6. Conclusion

In this work, we revisit hallucination in vision–language report generation from the perspective of intrinsic decoding biases in large language models. We propose a Layer-wise Expert-aligned decoding framework that integrates structured visual expert signals into intermediate representations of LLM, enabling adaptive correction of biased generation trajectories. By formulating generation as a step-wise expert-

guided refinement process and introducing a context-aware gated fusion mechanism, our method selectively aligns intermediate representations with fine-grained visual evidence while preserving linguistic coherence. Experiments compared with other methods demonstrate effective improvements in factual accuracy, with effective hallucination mitigation across different model scales and training settings. This work demonstrates that internal decoding guidance is critical as external constraints, offering a robust direction for eliminating hallucinations in medical report generation.

References

Babar, Z., van Laarhoven, T., and Marchiori, E. Encoder-decoder models for chest x-ray report generation perform no better than unconditioned baselines. *Plos one*, 16(11):e0259639, 2021.

Bai, S., Cai, Y., Chen, R., Chen, K., Chen, X., Cheng, Z., Deng, L., Ding, W., Gao, C., Ge, C., Ge, W., Guo, Z., Huang, Q., Huang, J., Huang, F., Hui, B., Jiang, S., Li, Z., Li, M., Li, M., Li, K., Lin, Z., Lin, J., Liu, X., Liu, J., Liu, C., Liu, Y., Liu, D., Liu, S., Lu, D., Luo, R., Lv, C., Men, R., Meng, L., Ren, X., Ren, X., Song, S., Sun, Y., Tang, J., Tu, J., Wan, J., Wang, P., Wang, P., Wang, Q., Wang, Y., Xie, T., Xu, Y., Xu, H., Xu, J., Yang, Z., Yang, M., Yang, J., Yang, A., Yu, B., Zhang, F., Zhang, H., Zhang, X., Zheng, B., Zhong, H., Zhou, J., Zhou, F., Zhou, J., Zhu, Y., and Zhu, K. Qwen3-vl technical report. *arXiv preprint arXiv:2511.21631*, 2025.

Banerjee, S. and Lavie, A. Meteor: An automatic metric for mt evaluation with improved correlation with human judgments. In *Proceedings of the acl workshop on intrinsic and extrinsic evaluation measures for machine translation and/or summarization*, pp. 65–72, 2005.

Chambon, P., Delbrouck, J.-B., Sounack, T., Huang, S.-C., Chen, Z., Varma, M., Truong, S. Q., Chuong, C. T., and Langlotz, C. P. Chexpert plus: Augmenting a large chest x-ray dataset with text radiology reports, patient demographics and additional image formats. *arXiv preprint arXiv:2405.19538*, 2024.

Chen, J., Tian, J., Zheng, T., Hui, Y., and Li, Z. Qwen-aec: Instruction-tuning large language models for high-performance building code analysis. *Advanced Engineering Informatics*, 71:104268, 2026.

Chen, X., Zhang, Y., Liu, Q., Wu, J., Zhang, F., and Tan, T. Mixture of decoding: An attention-inspired adaptive decoding strategy to mitigate hallucinations in large vision-language models. *arXiv preprint arXiv:2505.17061*, 2025.

Chen, Z., Song, Y., Chang, T.-H., and Wan, X. Generating radiology reports via memory-driven transformer. In *Proceedings of the 2020 Conference on Empirical Methods in Natural Language Processing (EMNLP)*, pp. 1439–1449, 2020.

Chen, Z., Shen, Y., Song, Y., and Wan, X. Cross-modal memory networks for radiology report generation. In *Proceedings of the 59th annual meeting of the association for computational linguistics and the 11th international joint conference on natural language processing (volume 1: long papers)*, pp. 5904–5914, 2021.

Deng, N. and Mihalcea, R. Rethinking table instruction tuning. *arXiv preprint arXiv:2501.14693*, 2025.

Grattafiori, A., Dubey, A., Jauhri, A., Pandey, A., Kadian, A., Al-Dahle, A., Letman, A., Mathur, A., Schelten, A., Vaughan, A., et al. The llama 3 herd of models. *arXiv preprint arXiv:2407.21783*, 2024.

Gu, D., Gao, Y., Zhou, Y., Zhou, M., and Metaxas, D. Radalign: Advancing radiology report generation with vision-language concept alignment. In *International Conference on Medical Image Computing and Computer-Assisted Intervention*, pp. 484–494. Springer, 2025.

Hou, W., Cheng, Y., Xu, K., Li, H., Hu, Y., Li, W., and Liu, J. Radar: Enhancing radiology report generation with supplementary knowledge injection. *arXiv preprint arXiv:2505.14318*, 2025.

Hu, E. J., Shen, Y., Wallis, P., Allen-Zhu, Z., Li, Y., Wang, S., Wang, L., Chen, W., et al. Lora: Low-rank adaptation of large language models. *ICLR*, 1(2):3, 2022.

Huang, X., Han, Y., Li, R., Wu, P., Zhang, K., et al. Cmeaa: Cross-modal enhancement and alignment adapter for radiology report generation. In *Proceedings of the 31st International Conference on Computational Linguistics*, pp. 8546–8556, 2025.

Huang, Z., Zhang, X., and Zhang, S. Kiut: Knowledge-injected u-transformer for radiology report generation. In *Proceedings of the IEEE/CVF conference on computer vision and pattern recognition*, pp. 19809–19818, 2023.

Irvin, J., Rajpurkar, P., Ko, M., Yu, Y., Ciurea-IIcus, S., Chute, C., Marklund, H., Haghgoo, B., Ball, R., Shpanskaya, K., et al. Chexpert: A large chest radiograph dataset with uncertainty labels and expert comparison. In *Proceedings of the AAAI conference on artificial intelligence*, volume 33, pp. 590–597, 2019.

Jiang, Y., Chen, C., Nguyen, D., Mervak, B. M., and Tan, C. Gpt-4v cannot generate radiology reports yet. In *Findings of the Association for Computational Linguistics: NAACL 2025*, pp. 2127–2154, 2025.

Johnson, A. E., Pollard, T. J., Berkowitz, S. J., Greenbaum, N. R., Lungren, M. P., Deng, C.-y., Mark, R. G., and Horng, S. Mimic-cxr, a de-identified publicly available database of chest radiographs with free-text reports. *Scientific data*, 6(1):317, 2019.

Kapadnis, M., Patnaik, S., Nandy, A., Ray, S., Goyal, P., and Sheet, D. Serpent-vlm: self-refining radiology report generation using vision language models. In *Proceedings of the 6th Clinical Natural Language Processing Workshop*, pp. 283–291, 2024.

Li, C., Wong, C., Zhang, S., Usuyama, N., Liu, H., Yang, J., Naumann, T., Poon, H., and Gao, J. Llava-med: Training a large language-and-vision assistant for biomedicine in one day. *Advances in Neural Information Processing Systems*, 36:28541–28564, 2023.

Li, Z., Wu, X., Du, H., Liu, F., Nghiem, H., and Shi, G. A survey of state of the art large vision language models: Benchmark evaluations and challenges. In *Proceedings of the Computer Vision and Pattern Recognition Conference*, pp. 1587–1606, 2025.

Lin, C.-Y. Rouge: A package for automatic evaluation of summaries. In *Text summarization branches out*, pp. 74–81, 2004.

Liu, C., Tian, Y., and Song, Y. A systematic review of deep learning-based research on radiology report generation. *arXiv preprint arXiv:2311.14199*, 2023.

Liu, C., Tian, Y., Chen, W., Song, Y., and Zhang, Y. Bootstrapping large language models for radiology report generation. In *Proceedings of the AAAI Conference on Artificial Intelligence*, volume 38, pp. 18635–18643, 2024a.

Liu, H., Xue, W., Chen, Y., Chen, D., Zhao, X., Wang, K., Hou, L., Li, R., and Peng, W. A survey on hallucination in large vision-language models. *arXiv preprint arXiv:2402.00253*, 2024b.

Liu, J., Tian, Y., and Song, Y. Balanced training data augmentation for aspect-based sentiment analysis. *arXiv preprint arXiv:2507.09485*, 2025a.

Liu, K., Ma, Z., Kang, X., Li, Y., Xie, K., Jiao, Z., and Miao, Q. Enhanced contrastive learning with multi-view longitudinal data for chest x-ray report generation. In *Proceedings of the Computer Vision and Pattern Recognition Conference*, pp. 10348–10359, 2025b.

Nicolson, A., Dowling, J., and Koopman, B. Improving chest x-ray report generation by leveraging warm starting. *Artificial intelligence in medicine*, 144:102633, 2023.

Qin, H. and Song, Y. Reinforced cross-modal alignment for radiology report generation. In *Findings of the Association for Computational Linguistics: ACL 2022*, pp. 448–458, 2022.

Sloan, P., Clatworthy, P., Simpson, E., and Mirmehdi, M. Automated radiology report generation: A review of recent advances. *IEEE Reviews in Biomedical Engineering*, 18:368–387, 2024.

Smit, A., Jain, S., Rajpurkar, P., Pareek, A., Ng, A. Y., and Lungren, M. P. Chexbert: combining automatic labelers and expert annotations for accurate radiology report labeling using bert. *arXiv preprint arXiv:2004.09167*, 2020.

Su, C., Tian, Y., Song, Y., and Zhang, Y. Text reinforcement for multimodal time series forecasting. *arXiv preprint arXiv:2509.00687*, 2025a.

Su, J., Chen, J., Li, H., Chen, Y., Qing, L., and Zhang, Z. Activation steering decoding: Mitigating hallucination in large vision-language models through bidirectional hidden state intervention. In *Proceedings of the 63rd Annual Meeting of the Association for Computational Linguistics (Volume 1: Long Papers)*, pp. 12964–12974, 2025b.

Sun, L., Zhao, J. J., Han, W., and Xiong, C. Fact-aware multimodal retrieval augmentation for accurate medical radiology report generation. In *Proceedings of the 2025 Conference of the Nations of the Americas Chapter of the Association for Computational Linguistics: Human Language Technologies (Volume 1: Long Papers)*, pp. 643–655, 2025.

Tanno, R., Barrett, D. G., Sellergren, A., Ghaisas, S., Dathathri, S., See, A., Welbl, J., Lau, C., Tu, T., Azizi, S., et al. Collaboration between clinicians and vision-language models in radiology report generation. *Nature Medicine*, 31(2):599–608, 2025.

Tian, Y. and Song, Y. Feature decomposition via shared low-rank matrix recovery for ct report generation. *IEEE Transactions on Medical Imaging*, pp. 1–1, 2025.

Tian, Y., Xia, F., and Song, Y. Diffusion networks with task-specific noise control for radiology report generation. In *Proceedings of the 32nd ACM International Conference on Multimedia*, pp. 1771–1780, 2024.

Tian, Y., Yan, Z., Lyu, N., and Song, Y. Extractive radiology reporting with memory-based cross-modal representations. *IEEE Transactions on Medical Imaging*, pp. 1–1, 2025.

Touvron, H., Martin, L., Stone, K., Albert, P., Almahairi, A., Babaei, Y., Bashlykov, N., Batra, S., Bhargava, P., Bhosale, S., et al. Llama 2: Open foundation and fine-tuned chat models. *arXiv preprint arXiv:2307.09288*, 2023.

Tu, T., Azizi, S., Driess, D., Schaekermann, M., Amin, M., Chang, P.-C., Carroll, A., Lau, C., Tanno, R., Ktena, I., et al. Towards generalist biomedical ai. *Nejm Ai*, 1(3): A10a2300138, 2024.

Vedantam, R., Lawrence Zitnick, C., and Parikh, D. Cider: Consensus-based image description evaluation. In *Proceedings of the IEEE conference on computer vision and pattern recognition*, pp. 4566–4575, 2015.

Wang, X., Li, Y., Wang, F., Wang, S., Li, C., and Jiang, B. R2gencsr: Retrieving context samples for large language model based x-ray medical report generation. *arXiv preprint arXiv:2408.09743*, 2024.

Wang, X., Wang, F., Li, Y., Ma, Q., Wang, S., Jiang, B., and Tang, J. Cxpmrg-bench: Pre-training and benchmarking for x-ray medical report generation on chexpert plus dataset. In *Proceedings of the Computer Vision and Pattern Recognition Conference*, pp. 5123–5133, 2025a.

Wang, Y., Sun, Y., Tan, T., Hao, C., Cui, Y., Su, X., Xie, W., Shen, L., and Yu, Z. Trrg: Towards truthful radiology report generation with cross-modal disease clue enhanced large language models. In *International Conference on Medical Image Computing and Computer-Assisted Intervention*, pp. 647–657. Springer, 2025b.

Wang, Z., Liu, L., Wang, L., and Zhou, L. R2gengpt: Radiology report generation with frozen llms. *Meta-Radiology*, 1(3):100033, 2023.

Wang, Z., Tian, Y., Wang, H., and Song, Y. Explainable multimodal aspect-based sentiment analysis with dependency-guided large language model. *arXiv preprint arXiv:2601.06848*, 2026.

Wu, J., Ding, Y., Liu, G., Xia, T., Huang, Z., Sui, D., Liu, Q., Wu, S., Wang, L., and Tan, T. Sharp: Steering hallucination in lvlms via representation engineering. In *Proceedings of the 2025 Conference on Empirical Methods in Natural Language Processing*, pp. 14357–14372, 2025.

Zhang, Y., Li, M., Long, D., Zhang, X., Lin, H., Yang, B., Xie, P., Yang, A., Liu, D., Lin, J., et al. Qwen3 embedding: Advancing text embedding and reranking through foundation models. *arXiv preprint arXiv:2506.05176*, 2025.